Simultaneous etching and oxidation of vicinal Si(100) surfaces: Atomistic lattice-gas modeling of morphological evolution

Marvin A. Albao,[1,2] Da-Jiang Liu,[1] Mark S. Gordon,[1,3] and J. W. Evans[1,4]
[1]*Ames Laboratory—U.S. Department of Energy, Iowa State University, Ames, Iowa, 50010, USA*
[2]*Department of Physics and Astronomy, Iowa State University, Ames, Iowa, 50010, USA*
[3]*Department of Chemistry, Iowa State University, Ames, Iowa, 50010, USA*
[4]*Department of Mathematics, Iowa State University, Ames, Iowa, 50010, USA*
(Received 26 July 2005; published 18 November 2005)

Exposure of a vicinal Si(100) surface to oxygen at about 10^{-8} Torr for temperatures between about 500 and 700 °C produces etching-mediated step recession in competition with oxide island formation. Furthermore, the oxide islands can locally pin the receding steps and thus produce complex surface morphologies. An atomistic lattice-gas model is developed to describe these processes which accounts for the complex interplay between the oxygen surface chemistry and the silicon surface and step dynamics. The oxygen related-processes include dissociative adsorption, diffusion, oxide formation, and etching via SiO desorption. The silicon surface processes include: conversion of single vacancies formed by etching to divacancies and Si adatoms, anisotropic diffusion and aggregation (primarily at step edges) of these divacancies and Si adatoms, and Si ad-dimer attachment-detachment dynamics at steps which reflects anisotropic energetics. Kinetic Monte Carlo simulation of this model allows characterization of the evolving step morphologies. Steps retain some qualitative features of their equilibrium structure, i.e., alternating rough S_B steps and smooth S_A steps, although etching tends to produce step pairing, and pinning produces protruding "finger" morphologies. These morphological features are seen in scanning tnneling microscopy studies. We also comment on other aspects of evolution such as a mixed pit nucleation and step flow mode, and compare behavior with step flow type growth during Si molecular beam epitaxy.

DOI: 10.1103/PhysRevB.72.195420 PACS number(s): 81.65.Cf, 68.35.Fx, 68.47.Fg, 68.55.Ac

I. INTRODUCTION

Molecular oxygen can react with various surfaces of silicon to produce etching, described by the mechanism $\mathrm{Si(solid)}+\frac{1}{2}\mathrm{O_2(gas)}\rightarrow\mathrm{SiO(gas)}+\mathrm{surface\ vacancy}$. Alternatively, it can react to produce surface oxide formation, described by $\mathrm{Si(solid)}+\mathrm{O_2(gas)}\rightarrow\mathrm{SiO_2(solid)}$.[1] At high surface temperatures (T), the lifetime of surface oxygen is small since SiO desorption is rapid, and etching of the surface or "active oxidation" dominates.[1,2] At low T, SiO desorption is inhibited or inoperative and the formation of the surface oxide predominates. Since the existence of oxide islands on the surface passivates or masks the underlying Si from etching, this regime is also described as "passive oxidation."[1,3] For moderate T, there is a transition regime involving competition between both etching and oxide formation which can lead to complex surface morphologies.[4–9] Behavior also depends somewhat on oxygen pressure, these regimes and the transition between them shifting to lower temperatures for lower pressures. The transition regime occurs at around 500–700 °C for oxygen pressures of about 10^{-8} Torr.[5]

For studies on perfectly flat low-index Si(100) or Si(111) surfaces, or on slightly miscut low-index surfaces where the terrace widths far exceed relevant diffusion lengths, initial exposure to oxygen at higher T leads to the nucleation and growth of monolayer deep etch pits.[1,2,6,8,10,11] This process is believed to be mediated by the formation, diffusion and subsequent aggregation of surface vacancies.[2,10,11] Continued exposure to oxygen leads to coalescence of these etch pits, and ultimately to pit formation in lower layers, i.e., to multilayer etching. This picture should apply generally to other surfaces of silicon.[12] In the transition regime at lower T, oxide islands are also formed which protect the underlying substrate from etching. Thus, prolonged etching leads to the formation of cone-shaped Si nanoprotrusions as multiple layers surrounding these oxide islands are etched away.[7,8]

Typical silicon (100) or (111) surfaces are not perfectly flat, but rather vicinal having a significant miscut angle relative to the (100) or (111) orientations. Such vicinal surfaces exhibit a staircase morphology being crossed by a somewhat periodic array of steps.[4,13,14] Etching of such surfaces can produce step recession, during which it is commonly believed that the vacancies resulting from etching diffuse to and erode step edges.[4,5,10,12] This picture is consistent with that above of vacancy-diffusion mediated etch pit formation on flat surfaces. At high T, etching could potentially result in a pure step flow regime, but at lower T etching can also produce nucleation and growth of vacancy etch pits at least on broader terraces.[7] Simultaneous formation of oxide islands in the transition regime at lower T produces pinning centers which interfere with this step recession process, and result in the creation of protruding "fingers."[4,5] Many of these features are revealed in scanning tunneling microscopy (STM) studies.[4–7,12] As an aside, it should be noted that some of the features described above for step-flow etching should have analogues for step-flow growth on Si surfaces during Si molecular beam epitaxy (MBE).[14] Since step-flow growth has been analyzed in detail both in experiment and atomistic modeling,[14] some comparison is appropriate of these previous studies with the current analysis of behavior during etch-

ing. We emphasize, however, that description of the etching process is significantly more complex at the atomistic level.

The above observations motivate us to develop an atomistic lattice-gas model which can describe the basic features of simultaneous etching and oxidation on vicinal Si(100) surfaces. Such modeling should include a realistic description of key surface diffusion processes (especially for surface vacancies) which impacts the evolution of nonequilibrium surface morphologies. This feature was not emphasized in previous modeling.[6] Our goal is to elucidate the complex interplay between the surface chemistry of etching and oxidation, and the Si(100) surface and step dynamics. The output of the model as determined by kinetic Monte Carlo (KMC) simulation (see Appendix A) will be a detailed characterization of the evolution of nonequilibrium surface morphology of the etched vicinal surface, which can be compared against experimental STM observations. In Sec. II, we first provide further background and details on the key surface processes operating in the rather complex oxygen+Si(100) system. Then, in Sec. III, we describe the ingredients of our atomistic lattice-gas model. Some benchmarking analysis of the behavior of this model for a flat (singular) Si(100) surface, as well as associated parameter determination, is presented in Sec. IV. Then, in Sec. V, we present results from our simulation studies for the etched surface morphology of vicinal Si(100). Finally, we offer some further discussion and a summary of our findings in Sec. VI.

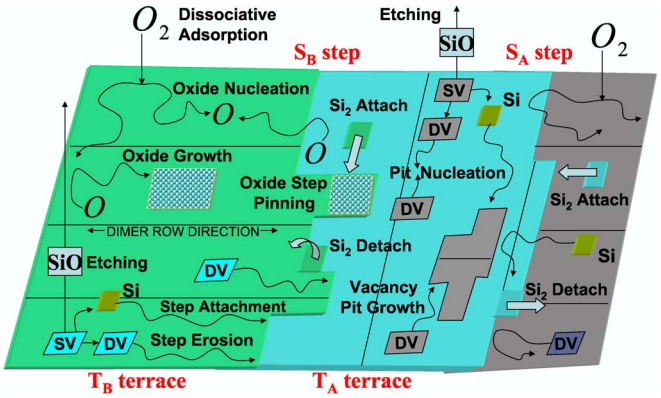

FIG. 1. (Color online) Schematic of key atomistic processes involved in the etching and oxidation of vicinal Si(100) and incorporated into our LG modeling: dissociative adsorption of O_2 (gas), nucleation and growth oxide islands mediated by O diffusion, etching by desorption of SiO to create single vacancies (SV), which convert to divacancies (DV) and Si adatoms, erosion of steps and possible formation of vacancy pits mediated by DV diffusion; pinning of receding steps by oxide islands, and attachment and detachment of Si ad-dimers at step edges. Adjacent terraces (descending from left to right) are separated by monoatomic steps. The alternating direction of the Si dimers rows (corresponding to the preferred direction of diffusion of DV's, Si adatoms and ad-dimers) is indicated by thin straight lines.

II. FURTHER CHARACTERIZATION OF THE VICINAL Si(100)+OXYGEN SYSTEM

A comprehensive characterization of the vicinal Si(100)+oxygen system, which can guide the development of our atomistic lattice-gas (LG) model, involves specification of both the vicinal Si(100) surface structure and dynamics, as well as the oxygen surface chemistry. Both of these are described in detail below and indicated schematically in Fig. 1.

Equilibrium structure and dynamics of vicinal Si(100) surfaces. The clean Si(100) surface reconstructs so that Si surface atoms pair to form dimers, thereby reducing the number of dangling bonds from two to one per atom. These surface dimers are aligned side-to-side in rows, the direction of which (indicated by the thin lines in Fig. 1) alternates between consecutive terraces separated by monatomic steps.[13,14] This feature of surface structure, and the tendency for etching to create divacancies (as described below), means that the dimer is the natural building block for the description of surface structure in our lattice-gas model, see Sec. III.

One particularly significant feature of the Si(100) surface is a strong anisotropy in the attractive interactions between surface dimers: the interaction between adjacent dimers within the same dimer row is much stronger than between adjacent dimers in neighboring dimer rows.[13] This interaction anisotropy implies a high kink creation energy on so-called S_A steps which run parallel to the dimer rows on the upper terrace bordering the step. This is because creation of kinks on S_A steps corresponds to breaking "strong bonds" between dimers in the same row. (Here, we are using the terms "bonds" in the sense of interactions in a lattice-gas model, rather than implying strong chemical bonds.) Likewise, this anisotropy implies a low kink creation energy for S_B steps which run orthogonal to dimer rows, as kink creation on S_B steps corresponds to breaking "weak bonds" between dimers in neighboring rows. Consequently, this anisotropy in kink creation energies leads to the well-known feature of alternating rough or meandering S_B steps, and smooth or nearly straight S_A steps, on a vicinal Si(100) surface.[13] Given these two different types of steps, it is conventional to distinguish two distinct types of terraces: T_A terraces are those above S_A steps for which the dimer rows run along the direction of the terrace; T_B terraces are those above S_B steps for which the dimer rows runs across the terrace.

It should also be noted that the interaction anisotropy implies a low step energy for S_A steps reflecting the feature that only "weak bonds" between dimers in neighboring rows need to be broken to create the step. It also implies a high step energy for S_B steps since "strong bonds" between dimers in the same row must be broken in creating the step. This impacts the equilibrium shape of adatom islands[15] or vacancy pits[16] on the Si(100) surface. Both tend to be elliptical with their longer sides oriented in the direction of the low-energy S_A steps. This observation is relevant for our studies, since etching can produce vacancy pits.

A detailed description of local equilibrium step structure on Si(100) should also reflect the feature that kinked steps are for the most part composed of units of pairs of dimers, so kink heights are mostly in multiples of $2a$ (where a denotes the lattice constant of the unreconstructed surface). Furthermore, the dominant mass-transport mechanism facilitating equilibration at step edges is often assumed to involve de-

tachment and reattachment, effectively in units of pairs of dimers. Thus, several previous modeling studies focused on equilibrium step structure and dynamics were based on attachment-detachment of dimer pairs subject to anisotropic nearest-neighbor interactions, but also including weaker longer range next-neighbor interactions or additional corner energies.[13,17] However, the basic features of nonequilibrium mesoscale step, island, or pit structure and dynamics, which are of relevance in our study, can be effectively captured by other modeling formulations, see Sec. III.

Interaction of oxygen with the Si(100) surface. Molecular oxygen absorbs dissociatively on the Si(100) surface. The constituent O adatoms do not immediately nucleate an oxide island, but rather typically separate via thermal surface diffusion.[1,8] This suggests that two adjacent O adatoms do not form a stable nucleus for an oxide cluster, i.e., the critical size (measured by the number of O atoms) above which oxide clusters are stable exceeds unity. In other words, the nucleation of oxide islands, which is mediated by diffusion of O adatoms, is reversible at typical surface temperatures.[8] There have been several studies of oxide nucleation following exposure to H_2O,[18,19] and after exposure to oxygen at lower T where there is a high O-adatom buildup.[20] However, the behavior in the regime of interest for this study is likely rather different.

Some detailed insights into the oxygen adsorption and etching energetics have been obtained from *ab initio* surface-integrated-molecular-orbital–molecular-mechanics (SIMOMM) analyses.[21,22] In this approach, a cluster of Si substrate atoms surrounding the adsorption or etching site is treated with high-level MO methods, and this cluster is embedded in a larger region treated at a much lower MM level. Such an analysis of the O+Si(100) system supports the previous density functional theory (DFT) studies[23] which indicated that there are multiple configurations of strongly adsorbed surface O which can rapidly interconvert.[22] These are naturally treated collectively as a single adsorbed state in our modeling. The SIMOMM analysis[22] also finds no evidence for a distinct weakly adsorbed species often postulated to mediate etching, a feature incorporated into previous "dual species" modeling,[1,7,9] but not in our "single-species" modeling. The barrier for surface diffusion for O adatoms has not yet been directly calculated from SIMMOM. However, studies for local motion of O between different adsorption sites suggest a diffusion barrier in the range 2.0–2.5 eV, which is consistent with earlier DFT studies.[18]

The desorption barrier for SiO is the key parameter controlling the transition from active to passive oxidation upon lowering T. Estimates in the literature range from ~2 (Ref. 2) to ~4 eV (Ref. 1) with SIMOMM predicting a value closer to 4 eV for a perfect surface.[22] When a single O adatom reacts with (i.e., etches) a defect-free portion of the flat Si(100) surface by desorbing as a volatile SiO species,[1] a single vacancy (SV) is created. This SV is believed to quickly convert to a divacancy (DV) by ejecting the remaining single unpaired Si atom up onto the Si(100) surface.[24] Thus, etching creates both DV's and single Si adatoms, the surface diffusion dynamics of which will be described in Sec. III.

We should also emphasize that SIMOMM indicates substantially lower barriers for SiO desorption resulting from reaction of O with Si which are not paired in a surface dimer.[22] This would include reaction of O with Si adatoms created from previous etching events when the SV formed by etching converts to a DV. The barrier for reaction of O with an Si ad-dimer is also plausibly lower than for reaction with a dimer embedded in a defect-free portion of the Si(100) surface, an issue pursued in Appendix B.

III. LATTICE-GAS MODEL FOR THE VICINAL Si(100) +OXYGEN SYSTEM

In this work, we implement a lattice-gas (LG) model to describe the numerous aspects of etching and oxidation of vicinal Si(100). Below, we separately describe the components of the model pertaining to the silicon surface dynamics, and to the oxygen surface chemistry. The KMC simulation algorithm used to implement this model is described briefly in Appendix A. Some refinements to the model described below are discussed in Appendix B. Most simulation results presented in this paper will correspond to a surface temperature of 550 °C. This temperature is chosen somewhat below that of most available experimental data at 600 °C (or above). This is because we wish to enhance the oxide island density to induce the pinning effects of interest in the early stages of etching which are more readily accessible to simulation.

Dynamics of the Si(100) surface. Our atomistic LG modeling is designed to capture the mesoscale features of surface morphology described above in Sec. II. One could consider building the LG model using one of three possible types of basic units. (i) Individual Si atoms which would provide the most flexibility, but this level of detail is unnecessary for our study (see below). (ii) Si dimers which is a particularly natural choice for our study since a key surface species created by etching is a divacancy. Si adatoms also generated by etching will be treated as a separate species (see below). (iii) Pairs of dimers as often used for studies of equilibrium structure, since this automatically produces the propensity for double-height kinks. This propensity, while likely diminished for nonequilibrium etching, could be reproduced in a model based on single dimers (where detachment of one dimer is quickly followed by that of a second). However, it is not essential to incorporate this local feature of step structure given that the mesoscale step structure of primary interest in our study. Furthermore, it is not so convenient to treat the key surface divacancy species in approach (iii).

Thus, in our type (ii) modeling, the Si(100) surface is regarded as built up of Si ad-dimers, and these are located at the sites of a regular simple cubic lattice. We must specify the orientation of the dimer rows which alternates between adjacent layers. We assume anisotropic lateral interactions between nearest-neighbor dimer units: a strong attraction $\phi_s > 0$ between dimers in the same row (i.e., in the direction parallel to the dimer rows), and a weak attraction $\phi_w > 0$ between dimers in adjacent rows (i.e., in the direction orthogonal to the dimer rows). These interactions will be selected as $\phi_s \approx 0.4$ eV and $\phi_w \approx 0.1$ eV so that our model

mimics the mesoscale equilibrium step structure on vicinal Si(100), see Sec. IV.

Our model incorporates detachment, terrace diffusion, and reattachment of Si dimers at step edges with hop rates assumed to have Arrhenius form $h_{Si2}=\nu_{Si2}\exp(-\beta E_{Si2})$. Here, $\beta=1/(k_BT)$ denotes the inverse temperature, the attempt frequency is chosen as $\nu_{Si2}=10^{12}$/s, and E_{Si2} denotes the direction-dependent activation barrier (which also depends on the local configuration, as described below). Terrace diffusion of an Si ad-dimer is described by a barrier of $E_{Si2}=E_d$, where $E_d=E_{df}=1.0$ eV for "fast" hopping along the dimer rows, and $E_d=E_{ds}=1.3$ eV for "slow" hopping orthogonal to these rows.[25,26] Barriers for intralayer detachment at step edges are chosen as $E_{Si2}=E_d+n_w\phi_w+n_s\phi_s$. Here, n_w denotes the number of in-layer neighbors in adjacent dimers rows, and n_s the number in the same row, prior to detachment, and E_d is chosen according to the direction of hopping. This type of Clarke-Vvedensky bond-counting model of activation barriers for surface diffusion[27] has been applied previously in studies of Si MBE where anisotropic interactions are also critical.[28]

Our modeling will also incorporate interlayer diffusion of dimers at step edges (i.e., hopping down of isolated dimers, or detachment from the step edge by hopping up onto the upper terrace). We adopt the same form for the barriers as described above for intralayer hopping except that we set $E_d=1/2(E_{df}+E_{ds})=1.15$ eV, an arbitrary but reasonable choice. Attachment rates and barriers for the reverse process are determined by detailed balance. Hops up and down multiple height steps are allowed.

The above generic bond-counting prescription of Si dimer hopping dynamics does allow DV formation at step edges, and DV diffusion via hopping of adjacent Si dimers into the DV location. The diffusion barrier for this indirect DV hopping process, as determined by the above bond-counting prescription, is either $E_{DV}=E_{df}+\phi_w+2\phi_s=1.9$ eV for hopping in the direction of the underlying dimer row or $E_{DV}=E_{ds}+2\phi_s+\phi_w=1.9$ eV for hopping orthogonal to the underlying dimer row. (This diffusion pathway just happens to be isotropic for our parameter choice.) However, the experimentally observed "fast" diffusion of divacancies is strongly anisotropic, with a significantly lower value of $E_{DVf}=1.7$ eV for hopping in the direction of the surface dimer row.[29] We thus refine the above generic prescription of silicon dynamics by incorporating an additional direct fast diffusion pathway for isolated DV's along dimer rows with rate $h_{DVf}=\nu_{DVf}\exp(-\beta E_{DVf})$. We use the observed barrier of $E_{DVf}=1.7$ eV and prefactor of $\nu_{DVf}=10^{16}$/s.[29] This special feature of our model deviating from generic bond counting is key to incorporating the appropriate diffusive transport kinetics for DV's. To preserve detailed-balance, this direct pathway is not operative for hops which destroy isolated vacancies such as incorporation at step edges or aggregation with other DV's.

We also do not allow surface dimers which are embedded in a terrace with coordination number of four to hop up onto the terrace. We assume that this process is rare, and as a result is not significant. Thus, we cannot allow the reverse process of filling of isolated DV's by diffusing dimers, as this would violate detailed-balance and corrupt the equilibrium structure of the model. This implies that DV's which diffuse to ascending steps cannot erode them, as the required "hopping up" of a DV corresponds to hopping down of a Si dimer to fill the DV. Thus, step erosion mediated by terrace diffusion of DV's occurs only at descending steps.

Interaction of oxygen with the Si(100) surface. In our atomistic LG model, molecular oxygen adsorbs dissociatively at a rate of $F=0.0016$/s per site on adjacent empty sites of the Si substrate, i.e., on sites not covered by adsorbed O or oxide. This rate corresponds roughly to an oxygen pressure of $P_{O2}=6\times10^{-8}$ Torr, where we assume that $F\approx2.7\times10^4 P_{O2}$.[8] Isolated O adatoms are assumed to diffuse isotropically to adjacent sites on the surface with hop rate $h_O=\nu_O\exp(-\beta E_{dO})$, where $E_{dO}=2.4$ eV and $\nu_O=10^{16}$/s.[18] An O adatom with one neighboring O can still hop, but with rate generally reduced from h_O by a factor r (typically set to unity here). However, O adatoms with two or more neighboring O's are regarded as immobilized into oxide islands. This is an idealized treatment of reversible formation of oxide islands, which, of course, neglects oxide structure. However, it will suffice to produce reasonable behavior for those features of oxide formation which are most relevant for our study, specifically the observed oxide island densities and the oxygen uptake kinetics (as discussed in Sec. IV).[8] In our modeling, we assume that O adatom hopping and oxide nucleation is insensitive to Si surface structure, i.e., O can hop across steps at the same rate as for terrace diffusion, and O on adjacent terraces with different heights can still participate in the formation of oxide islands.[8]

It is also possible for O adatoms to etch the underlying Si atoms to create desorbing SiO at rate $d_{SiO}=\nu_{SiO}\exp(-\beta E_{SiO})$, where we set $\nu_{SiO}=4\times10^{19}$/s,[1] and choose $E_{SiO}=3.23$ eV. The oxide island density is quite sensitive to the value of E_{SiO} which is chosen to roughly recover experimental observations, see Sec. IV. Each etching event involving a Si embedded in a terrace creates a SV, which in our modeling immediately converts to a DV and a Si adatom.[11] Occasionally, etching occurs by direct reaction with step edge dimers, which causes recession of the step edge plus a Si adatom. The diffusion dynamics for Si adatoms is described below, and that for DV's is described above. It should be emphasized that the diffusion of DV's to descending step edges produces recession of those step edges, and that a sufficient density of DV's on terraces of the vicinal surface can potentially result in nucleation and growth of etch pits.[10] Diffusion of Si adatoms to and attachment at step edges or vacancy pits partly counterbalances the step erosion or pit growth due to DV's, as discussed in more detail below.

Dynamics of Si adatoms and their reaction with O. The Si adatoms, which are created by conversion of SV's to DV's, diffuse along Si dimer rows with a low barrier of $E_{df}(\mathrm{Si})=0.67$ eV and across such rows with a higher barrier of $E_{ds}(\mathrm{Si})=1.0$ eV, both determined from experiment.[30] The prefactor for such hopping is chosen as $\nu_{Si}=10^{13}$/s.We assume that diffusing Si adatoms can cross portions of steps with S_A orientation without interaction, but they are adsorbed at steps with S_B orientation becoming part of the substrate. This "anisotropic sticking" feature is supported by various theoretical[31] and experimental[32,33] studies. In our model, when a Si adatom reaches a step with S_B orientation, it is

converted into a Si dimer at the step edge with probability 1/2, and removed with probability 1/2. This provides a simple way to treat aggregation which is on average consistent with mass conservation.

The feature that etching produces Si adatoms on the surface (as well as DV's) can potentially lead to the formation of Si adatom "regrowth islands" resulting from aggregation of these Si adatoms.[34] This process is expected to be significant at lower T around 300 °C,[34] but not at the higher T used in our study. In our modeling, we do however incorporate the irreversible aggregation of two Si adatoms to form a Si addimer. Also, Si adatoms can aggregate with dimers, or clusters of dimers, using the same rule with which we treat aggregation at step edges.

Finally, we discuss the scenario where a diffusing Si adatom meets a diffusing O adatom. In our modeling, instantaneous reaction is assumed to occur (unless stated otherwise), producing a SiO which immediately desorbs. The choice of instantaneous reaction is motivated by the SIMOMM analyses of SiO desorption barriers for unpaired Si atoms, as described in Sec. II.

Anisotropic accommodation at step edges. Although implicit in the above rules, it is appropriate to emphasize that certain features of our model imply effective anisotropic accommodation or incorporation of DV's at step edges. Perhaps the most obvious of these features is the anisotropic diffusion of DV's preferentially across T_B terraces together with constraint of incorporation only at descending step edges. These two features imply ready incorporation of DV's at the descending S_B steps bordering T_B terraces. In contrast, DV diffusion on T_A terraces is predominantly parallel to the descending S_A step edge bordering these terraces, so these S_A step edges are not readily reached and eroded. However, there is another source of anisotropy in DV accommodation, apart from the differing frequency of reaching descending step edges. When a DV reaches a step with S_B orientation, overall the system gains a "strong bond," versus a "weak bond" upon reaching a step with S_A orientation. This feature, deriving from anisotropic energetics, also implies anisotropic accommodation preferentially at S_B steps (at least in the regime of reversible attachment of DV's at step edges).

Finally, it should be noted that there is also an anisotropy in aggregation of Si adatoms at step edges (as in Si MBE) which partly counterbalances the anisotropy in recession associated with the DV's. This anisotropy for Si adatoms obviously follows since in our modeling, S_A steps are transparent to Si adatoms. These adatoms can incorporate at S_B steps from the upper or lower terrace, although the former should dominate due to anisotropic diffusion. Thus, the enhanced growth of S_B steps relative to S_A steps as a result of Si adatom aggregation will partly offset the enhanced erosion of S_B steps as a result of anisotropic DV accommodation. However, DV-mediated erosion should dominate since DV's and Si adatoms are created in equal numbers, but each DV removes two Si atoms from the step edge, whereas each Si adatom adds only one Si atom.

General comments on rate determination. As indicated above, wherever possible rates in our modeling are chosen based on available experimental (or theoretical) values. Extensive information is available for Si surface dynamics, but less is available for oxygen surface dynamics (e.g., there is considerable uncertainty in the value of E_O and the details of oxide nucleation). Some key barriers or interactions (e.g., E_{SiO}, and the effective Si ad-dimer interactions) are treated as free parameters and adjusted to match relevant observed experimental behavior. In some cases (e.g., SiO desorption or DV diffusion), prefactors reported in the literature (and adopted here) seem unusually high. This possibly reflects a "compensation effect" due to oversimplified analysis where both prefactors and barriers may be overestimated, but the rates are accurate. For our study focusing on 550C, reasonable estimation of the rates suffices.

Other modeling. It is appropriate to briefly compare our model described above with previous work. An atomistic model for etching and oxidation of vicinal Si(100) was developed in Ref. 6 based on units of individual Si atoms. This model incorporated a detailed description of the equilibrium structure of the vicinal Si(100) surface, even including antiphase boundaries on (100) terraces. These antiphase boundaries are ignored in our formulation, since these should not play a significant role during the etching process. Note that the treatment in Ref. 6 of the surface energetics is not geared to providing a precise description of the diffusive transport for various surface species such as divacancies. However, an accurate description of transport kinetics should be important in describing such features of the nonequilibrium surface morphology as the competition between step-flow etching, and nucleation and growth of etch pits on terraces. Hence, the focus of our model development is on an accurate description of surface diffusion. It should also be noted that the complexity of the description of the surface in Ref. 6, and limitations in computing resources at the time of that study, required that approximations be made in the simulation algorithm which changed the relative rates of various processes. In addition, the simulated system and feature sizes were much smaller than in experiment, which could affect some aspects of the morphological evolution such as finger formation and pinch off. These limitations are avoided in our study.

IV. MODEL BENCHMAKING: PARAMETER DETERMINATION, REACTION KINETICS, SILICON SURFACE MORPHOLOGY, AND EVOLUTION

The model analysis and parameter determination described first below focuses on reaction kinetics for oxidation and etching behavior on a flat (singular) Si(100) surface.

(i) *Determination of and sensitivity to SiO desorption barrier*. One requirement which we place on our model is to obtain realistic values for the oxide density N_{ox} for exposure of Si(100) surface to O_2 at a temperature of 550 °C (for which we present simulation results in this paper). Thus, to estimate N_{ox} at 550 °C, we use the experimental Arrhenius dependence of the oxide island nucleation rate above 600 °C.[7] Assuming that this dependence also applies to N_{ox}, we extrapolate measured values at higher T to obtain the value at 550 °C. This yields $N_{ox} \sim 3 \times 10^{-4}$ per surface atom for two monolayers (ML) etched at 550 °C. In fact, a similar value is obtained using our earlier atomistic model,[8] which

simplifies the Si surface dynamics, and which was fit to higher T data for N_{ox} We find that choosing $E_{SiO}=3.23$ eV (and $\nu_{SiO}=4\times10^{19}$/s) reasonably recovers this value (for reversible nucleation with $r=1$), whereas choosing, e.g., 3.20 eV produces significantly lower N_{ox}. Choosing a lower prefactor would yield a lower activation barrier to recover the same desorption rate and oxide nucleation behavior a 550 °C.

As an aside, we note that the diffusion length for O on the surface before desorption (as SiO) satisfies $L_O=(h_O\tau_O)^{1/2}$ where $\tau_O=1/d_{SiO}$ is the O lifetime on the surface. Under the above conditions at 550 °C, one has $L_O\approx5.5a$, far below the oxide island separation of $L_{ox}=(N_{ox})^{-1/2}\approx60a$. Thus, oxide island nucleation can be regarded as occurring in the regime of strongly "incomplete condensation:" the diffusing O species mediating oxide nucleation and growth typically desorb (as SiO) before reaching an oxide island.[8,35,36] Recognition of this feature provides some insight into the dependence of N_{ox} on key parameters such as E_O.[8] One caveat with the above analysis is that the value obtained for L_O is quite sensitive to the choice of prefactors and barriers for SiO desorption and for O diffusion, for which there is considerable uncertainty. In fact, some experiments suggest a significantly larger L_O.[37] However, provided that the desorption barrier for SiO exceeds the surface diffusion barrier for O (which is a reasonable assumption), then it is clear that L_O will decrease with increasing T.

(ii) *Interplay between oxide nucleation and SiO desorption rates*. The choice of oxide nucleation used above with $r=1$ is strongly reversible, the smallest stable cluster requiring four O adatoms. Potentially, by making nucleation more facile (i.e., by decreasing r towards 0, which corresponds to irreversible oxide island formation), one could still match the experimental N_{ox} by simultaneously decreasing E_{SiO} thereby reducing the lifetime of O on the surface. This would imply nonuniqueness in parameter selection. Indeed, the behavior of N_{ox} for $E_{SiO}=3.23$ eV and $r=1$ up to ~0.6 ML etched (choosing $T=530$ °C and $P_{O2}=2\times10^{-7}$ Torr) can be recovered using $E_{SiO}=3.08$ eV and $r=0.1$. However, we find that the oxygen uptake is much slower for the second choice, presumably because a significantly smaller lifetime τ_O and smaller diffusion length L_O for O on the surface inhibits oxide island growth, see Fig. 2. Thus, the requirement of producing reasonable behavior for both N_{ox} and the oxygen uptake does narrow the range of viable model parameters.

(iii) *Reaction of O with Si adatoms*. In Sec. III, we described why fast reaction is expected to occur between adsorbed O and Si adatoms. How significant is this reaction channel? To test this effect, we perform simulations with and without this channel operative (where for the former we assume instantaneous reaction). The comparison is shown in Fig. 3 for oxygen uptake at 550 °C and $P_{O2}=6\times10^{-7}$ Torr. As expected, uptake is somewhat slower with this reaction channel operative. However, a minor decrease in the value of E_{SiO} can recover the same behavior as with the channel inoperative.

Next, we discuss aspects of model analysis and parameter determination related to the Si surface, both the morphology of vicinal surface and the dynamics of etch pit formation.

(iv) *Mesoscale equilibrium step structure on a vicinal Si(100) surface*. Here, we determine effective values for Si dimer lateral interaction energies which will reasonably reproduce the observed step structure of vicinal surfaces. If $h(x)$ denotes the position or "height" of the step edge orthogonal to the direction, x, along the step, then the step structure is typically quantified by the correlation function[38]

$$G(x)=\langle[h(x+x_O)-h(x_O)]^2\rangle\approx(b^2/a)|x| \quad \text{for short separations } x. \tag{4.1}$$

Here, $\langle\ \rangle$ denotes a suitable average (e.g., over reference positions x_0 or over time, or over an ensemble of steps) and a is the surface lattice constant. This behavior is consistent with a random walk type picture of step wandering, where correspondingly b^2 is described as the step diffusivity. For larger

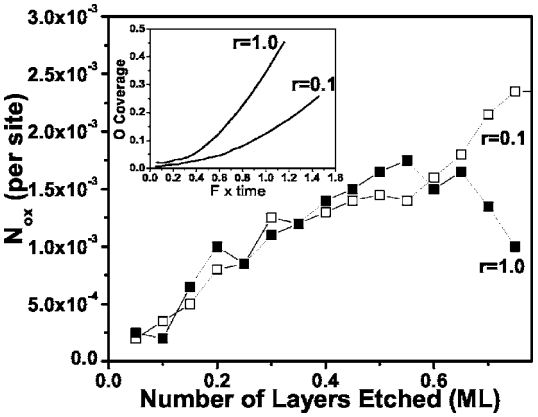

FIG. 2. Model predictions at 530 °C and $P_{O2}=2\times10^{-7}$ Torr for the oxide cluster density N_{ox} and oxygen uptake (inset) for two different parameter choices ($E_{SiO}=3.23$ eV, $r=1.0$) and ($E_{SiO}=3.08$ eV, $r=0.1$ eV). The O coverage is the total coverage from both oxide islands and isolated diffusing adatoms. These parameter choices are selected to give comparable initial behavior of N_{ox}. The decrease in N_{ox} for $r=1$ (compared to $r=0.1$) above 0.6 layers etched reflects coalescence effects (due to the larger oxide island area).

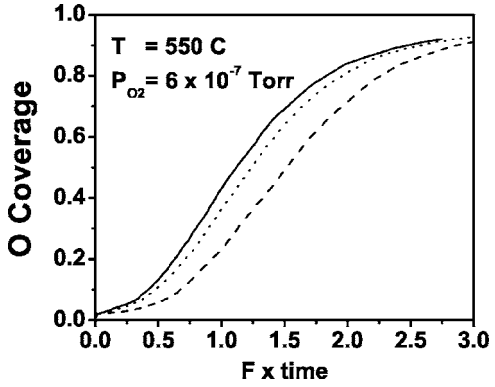

FIG. 3. Oxygen uptake curves showing the effect of reaction between O and Si adatoms. Again, the O coverage is the total coverage from both oxide islands and isolated diffusing adatoms. For comparison, cases are shown when the Si+O reaction is (i) "on" with $E_{SiO}=3.22$ eV (long dash), (ii) "off" with $E_{SiO}=3.22$ eV (short dash), and (iii) "off" with $E_{SiO}=3.25$ eV (solid line).

separations x along the step, growth of $G(x)$ saturates due to step-step interactions. The diffusivity is mainly controlled by the kink creation energies $\varepsilon_w=\phi_w/2$ and $\varepsilon_s=\phi_s/2$ for kinks on S_B steps and S_A steps, respectively. Within a terrace-step-kink model where the energy cost associated with kinks of height n is $E=|n|\varepsilon$, and ε is the relevant kink creation energy, it follows that[38]

$$b^2/a^2=\frac{1}{2}\sinh^{-2}(\beta\varepsilon) \tag{4.2}$$

which increases strongly with decreasing ε (i.e., diffusivity increases with greater ease of kink creation). The step diffusivity is quantified in STM images taken at room temperature, but presumed to reflect the equilibrium step structure which is "frozen in" at a higher temperature of about 500 °C.[13] The effective values of the kink creation energies $\varepsilon_w\approx 0.05$ eV and $\varepsilon_s\approx 0.2$ eV, are chosen so that our model roughly reproduces the "high" diffusivity of the S_B steps, and the "low" diffusivity of the S_A steps on an equilibrated vicinal surface.[13] These choices imply effective values for interactions of $\phi_w\approx 0.1$ eV and $\phi_s\approx 0.4$ eV, quoted in Sec. III.

(v) *Characterization of etch pit nucleation*. A traditional far-from-equilibrium picture[36,39] of etch pit nucleation ignores the equilibrium "background" density of DV's, and assigns a "small" critical size i such that a new stable etch pit is created by aggregation of $i+1$ diffusing DV's (which themselves are created by etching).[8] However, for high T, one cannot ignore the equilibrium density $n_{\mathrm{DV}}^{\mathrm{eq}}\sim\exp[-\beta(\phi_w+\phi_s)]$, of DV's created primarily by continual attachment-detachment at step edges. Specifically, for high T, the total density n_{DV} of DV's, which includes a supersaturation component due to etching, may not greatly exceed or may only slightly exceed $n_{\mathrm{DV}}^{\mathrm{eq}}$. If n_{DV} is only slightly above $n_{\mathrm{DV}}^{\mathrm{eq}}$, then a near-equilibrium formulation of etch pit nucleation is required.[40] Indeed for Si MBE on Si(100), nucleation of adatom islands is far from equilibrium with $i=1$ below 280 °C,[30] and near equilibrium around and above 650 °C.[40] As an aside, we note that high-T near-equilibrium behavior can sometimes be effectively mimicked by a far-from-equilibrium treatment with a small critical size.[40] Our previous treatment of etch pit nucleation at 770 °C was of this form.[8,11]

To explore this issue more completely, we have run simulations of etching for various temperatures and monitored the DV density n_{DV}. Then, n_{DV} is compared with the DV density in the absence of exposure to oxygen $n_{\mathrm{DV}}^{\mathrm{eq}}$. We find supersaturation in the presence of etching as characterized by $n_{\mathrm{DV}}/n_{\mathrm{DV}}^{\mathrm{eq}}\approx 20$, 8, and 3, at 500, 550, and 600 °C, respectively.[41] Thus, etch pit nucleation at or below 500 °C might be described as far from equilibrium, but neither this far-from-equilibrium picture nor a near-equilibrium picture applies at 600 °C. Etch pit nucleation should become near equilibrium by 770 °C.

V. RESULTS FOR MORPHOLOGICAL EVOLUTION DURING ETCHING OF VICINAL SI(100)

In Fig. 4, we present simulation results from our atomistic model for the evolution of surface morphologies during etching and oxidation of vicinal Si(100) at 550 °C. All images are 100×100 nm^2. The terraces are descending from right to left. First, Fig. 4(a) shows results for the equilibrium morphology in the absence of etching. Alternating rough S_B steps and smooth S_A steps are evident. Simulations confirm that steps become smoother at lower T, but behavior at 500 °C has changed little from 550 °C and matches well experimental observations shown, e.g., in Ref. 13. Next, in Figs. 4(b)–4(f), we show an etch sequence for $P_{\mathrm{O2}}=6\times 10^{-8}$ Torr corresponding to roughly 0.5, 1, 1.5, 2, and 2.5 layers of Si removed, respectively. Initially, the S_B steps recede much faster than the S_A steps, thus disrupting the approximate equilibrium balance between the populations or areas of the T_A and T_B terraces. The development of this imbalance is due to the anisotropic accommodation of DV's at step edges favoring S_B step recession, as described in Sec. III. After etching of about 1 layer, oxide islands have already formed and soon thereafter begin to pin recession of step edges. This is most obvious for S_B steps, which are not very stiff,[13,32] and which readily bend around oxide islands to form large protruding "fingers" after further etching. In other simulations, one can also find examples of "break-away" Si islands resulting when these fingers pinch off. There is some transient pinning of much stiffer S_A steps, but these tend to snap off more quickly at the pinning site rather than creating extended fingers. [Consider the large oxide cluster in the lower left of Fig. 4(d) around which an S_A step is bent. During etching of the next 0.5 ML, this step has broken away leaving behind a layer of Si under the oxide island, see Fig. 4(e). As oxide islands grow larger, pinch-off becomes more difficult.

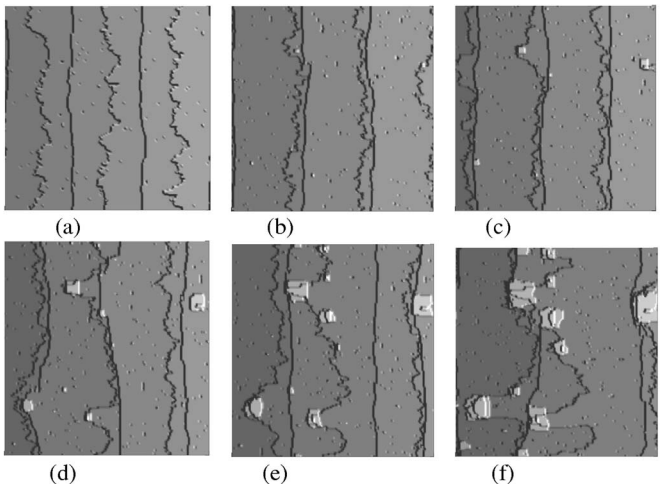

FIG. 4. Simulated images (100×100 nm^2) of vicinal Si(100) surface morphologies. (a) Equilibrium structure of vicinal Si(100) at 550 °C with terraces ascending from left to right separated by alternating rough S_B steps and smooth S_A steps. (b)–(f) Morphologies after etching of 0.5, 1, 1.5, 2, 2.5 layers of Si at 550 °C with $P_{\mathrm{O2}}=6\times 10^{-8}$ Torr. Note the rapid initial recession of S_B steps, and the subsequent pinning by oxide islands (shown as light colored regions).

During the surface evolution shown in Fig. 4, we have also monitored the ratio R of the areas of T_A to T_B terraces

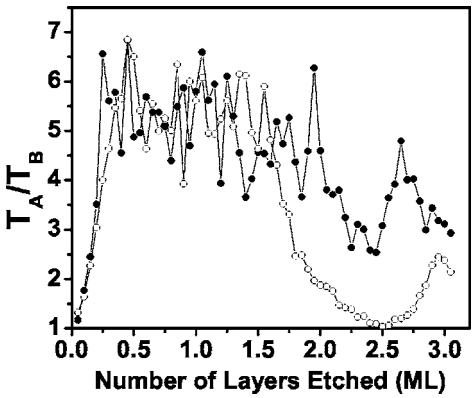

FIG. 5. Evolution of the ratio of the areas of T_A and T_B terraces versus number of layers etched at 550 °C with $P_{O2}=6\times10^{-8}$ Torr. Solid symbols are data is taken from the simulation of Fig. 4. Open symbols are data from an independent simulation. The initial increase is robust, but subsequent behavior is fluctuation dominated (for systems sizes of the order 100×100 nm^2), depending on the details of individual pinning events.

for etching at 550 °C with $P_{O2}=6\times10^{-8}$ Torr. This ratio at first increases quickly from its initial value of unity due to the more rapid recession of S_B steps. See the solid symbols in Fig. 5. This behavior is evident from inspection of Fig. 1(a), where the areas of T_A and T_B terraces or almost equal, compared with Figs. 4(b) and 4(c) where the T_B terraces (to the right of the rough S_B steps) are much narrower. It should also be noted that the initial degree of anisotropy in step propagation is close to the maximum possible where S_A steps are stationary. In this case, one has

$$R_{\max}=(1+2\theta_{\text{etch}})/(1-2\theta_{\text{etch}}) \text{ for } \theta_{\text{etch}}<0.5 \text{ ML etched.} \tag{5.1}$$

This result (5.1) assumes an initial $R=1$ and neglects fluctuations, so R values in our simulations can actually be larger. After etching of about one layer, the onset of step pinning by oxide clusters increases again the relative population of T_B terraces, reducing R towards unity. Thereafter, the behavior of R becomes more erratic (for system sizes considered here), as it depends on individual pinning events. To confirm this picture in which the initial rapid increase of R should be robust, but subsequent behavior more random, we show results of two independent simulation runs in Fig. 5.

Since anisotropy in propagation of S_B and S_A steps is a key feature of both etching and Si MBE, some further discussion and analysis is appropriate. In Sec. III, we noted that there are two components producing anisotropy in DV accommodation: anisotropic DV diffusion and anisotropic energetics. Their relative influence can be assessed by comparing step evolution with and without anisotropic DV diffusion (where, for the latter, we simply switch off the direct pathway for DV diffusion along dimer rows describe in Sec. III). Results shown in Fig. 6 reveal that recession of the S_B steps is significantly more rapid with anisotropic DV diffusion: $R\approx4$ with anisotropic diffusion, versus much smaller $R\approx1.7$ without anisotropic diffusion (for 0.25 ML etched). We

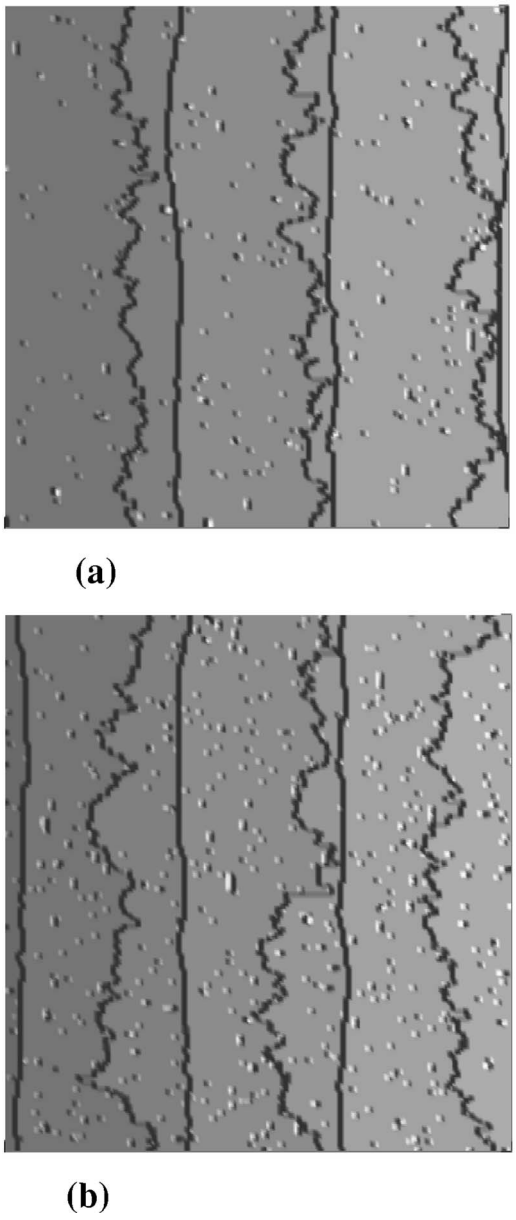

FIG. 6. Analysis of anisotropy in step recession after 0.25 layers etched at 550 °C with $P_{O2}=6\times10^{-8}$ Torr: (a) standard model of Fig. 4 with anisotropic DV diffusion and anisotropic Si dimer interactions where $R\approx4$ and (b) modified model with isotropic DV diffusion but retaining anisotropic interactions where $R\approx1.7$.

have checked the robustness of these results with additional simulations. It is clear from these results that the degree of anisotropy in step propagation will decrease smoothly with decreasing $h_{\text{DV}f}$. We should reiterate that step propagation is still anisotropic without anisotropic DV diffusion as a consequence of the effect of the anisotropic interactions. Finally, we have argued that anisotropic incorporation of Si adatoms should somewhat counterbalance the anisotropy in DV incorporation. To check this claim, we have run simulations for a modified model where the Si adatoms created by SV to DV conversion are immediately removed from the surface (rather than allowed to diffuse to steps). In this modified model, we find that the anisotropy in step propagation is somewhat en-

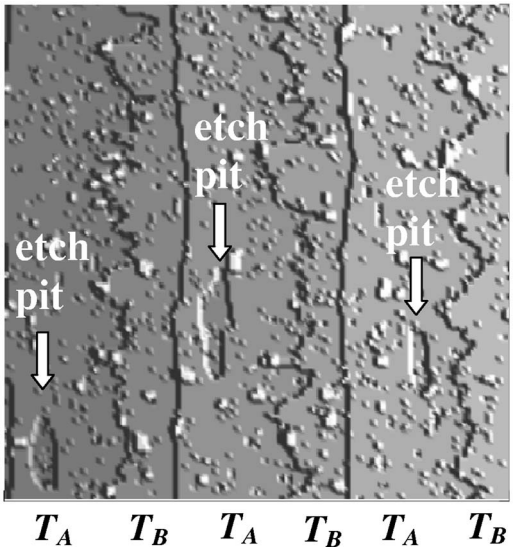

FIG. 7. Simulation image (100×100 nm^2) showing alternating formation of etch pits (indicated by arrows) on T_A terraces and step flow across T_B terraces at 550 °C and $P_{O2}=8\times10^{-7}$ Torr. Light colored regions are (small) oxide islands, which occur at higher density than in Fig. 4.

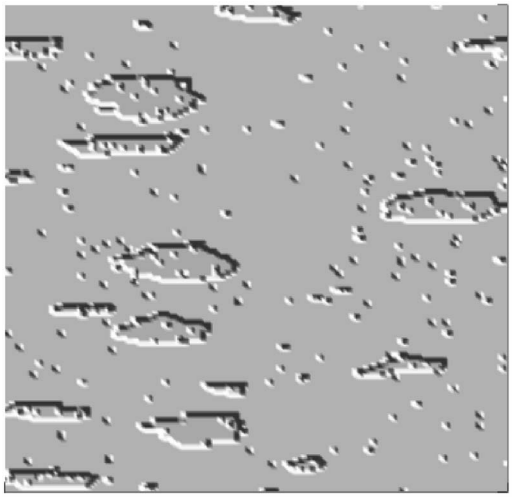

FIG. 8. Simulation image (100×100 nm^2) showing etching of a flat Si(100) surface at 550 °C with $P_{O2}=2\times10^{-8}$ Torr. The irregular etch pits are elongated along the dimer row direction (which is horizontal in this image).

hanced relative to the original model (as expected).

It is appropriate to explore the consistency of our model predictions and experimental observations for anisotropy in step propagation at higher temperature of 600 °C and a somewhat lower pressure of $P_{O2}=2\times10^{-8}$ Torr.[5] For these conditions, data from a single experimental run indicates an initial increase of R which is slower than that described above at 550 °C, with $R\approx2$ for 1/3 ML of Si etched (assuming that 1 ML etched corresponds to 63 Langmuirs exposure to oxygen).[5] Our model prediction of $R\approx2.5$ (with large fluctuations) for 1/3 ML of etched under these conditions is reasonably consistent with the experimental value (in contrast to the simulation result of $R\approx5$ at 550 °C, and $R_{max}=5$, for 1/3 ML etched as described above).

Next, we examine etching behavior again at 550 °C but for higher oxygen pressure $P_{O2}=8\times10^{-7}$ Torr which serves to enhance the formation of etch pits on terraces relative to step recession. Figure 7 shows a 100×100 nm^2 region of a vicinal Si(100) surface revealing a mixed pit-nucleation and step-flow etching mode. This mode involves an alternation between nucleation of etch pits on T_A terraces where the dimer rows are parallel to the steps, and pure step recession on T_B terraces where the dimer rows are orthogonal to the steps. This behavior should be expected since the DV density will grow higher on the former terraces where DV's cannot so easily reach and be incorporated at step edges, and thus nucleation of etch pits is enhanced. The etch pits tend to be aligned with the dimer rows, reflecting their preferred equilibrium elliptical structure.[15] Note that the oxygen higher pressure used in this simulation also produces a substantially higher density of oxide islands.

For completeness, in Fig. 8, we show simulation results for etching of a flat (singular) Si(100) surface purely by pit nucleation and growth also at 550 °C, but for lower $P_{O2}=2\times10^{-8}$ Torr to enhance pit size. In general, complete shape equilibration is not expected on the time scale of etching,[2,8,11] and shape fluctuations are significant. Consequently, pits somewhat irregular although still reflecting their equilibrium elliptical structure elongated in the direction of the dimer rows.[15] Such irregular pits have been seen in STM studies of etching on broad terraces.[10] We have already observed in Sec. IV that nucleation in this regime is intermediate between far-from-equilibrium and near-equilibrium. In addition, we should also note that the details of the nucleation behavior should be impacted by the strong anisotropy in DV diffusion.[42] Furthermore, growth behavior of individual pits is expected to be determined by their associated "capture zones"[2,11,43] from which they collect diffusing DV's. These capture zones will also reflect anisotropy in DV diffusion [which is presumably much weaker in previous studies at very high T (Refs. 2 and 11)].

The various features predicted by our simulation model are in fact apparent in STM studies of the etching of vicinal Si(100).[4,5] The initial preferential etching, i.e., faster recession, of S_B steps is clear, as is their pinning by some sort of defect site to create fingers and the subsequent break off of fingers. See particularly Figs. 1 and 2 in Ref. 4, and Fig. 1 in Ref. 5. Clear evidence is provided that the defect pinning sites are directly related to oxygen, and are thus reasonably identified as oxide islands.[4,5] The behavior of the ratio R of T_A to T_B terrace areas with exposure to oxygen at 600 °C (Ref. 5) is consistent with model predictions, as discussed above. An image of mixed-mode growth can be found in Ref. 12.

VI. DISCUSSION AND SUMMARY

Often etching or erosion processes are regarded as the inverse of growth. Thus, it is instructive to compare morphological evolution described above for etching of vicinal Si(100) with growth modes and morphologies for MBE of atomic Si on vicinal Si(100). One finds various growth re-

gimes for Si MBE.[14,29] (i) Island nucleation at low T of 300 °C. (ii) A mixed growth mode at 450 °C initially involving step flow of adatoms across T_B terraces to rapidly advancing S_B steps, and island nucleation on T_A terraces. (iii) Step flow at 500 °C and high flux, where S_B steps almost catch up to S_A steps creating near-double length T_B terraces separated by imperfect biatomic steps. Such steps are S_A-like in the sense that they cannot efficiently capture adatoms, so the adatom density builds up producing some island nucleation and a decrease in the relative population of T_B terraces. (iv) Pure step flow at 500 °C for low flux and at higher T, although perfect bistable steps do not form due to weak pinning effects (or due to entropic step repulsion, which is dominant above 580 °C).

Thus, the more rapid advance of S_B steps in MBE, and the corresponding enhancement of T_B relative to T_A terrace population, is analogous to behavior seen in etching. Step flow growth would be observed in etching at 550 °C or above (for lower P_{O2}) if not for the strong pinning effects of oxide islands. The weak pinning effects in MBE produce rather different "fatter finger" morphologies than in etching. Entropic step repulsion will also be significant for etching at high enough T. The mixed mode growth in MBE at 450 °C mimics that in etching at 550 °C for higher P_{O2}. The shift of these growth modes to higher T for etching (relative to MBE) reflects the larger activation barrier for DV diffusion relative to Si adatom diffusion.

More recent studies of Si MBE on Si(100) argue that anisotropic diffusion produces an effective inverse ES barrier which induces a step bunching instability.[44] Such subtle instabilities could in principle occur for etching, but in practice they do not have a chance to develop in our study as the surface morphology is dominated by strong pinning effects.

An even closer analogy with etching of Si(100) is provided by studies of step recession during ion sputtering of Si(100),[45] since sputtering produces surface vacancies which can nucleate vacancy pits at lower T, or diffuse to and erode steps at higher T. (Sputtering may produce other surface adspecies which play a role in surface evolution, although detailed characterization is not available.) For sputtering, faster retraction of S_B steps and dominance of T_A terraces is observed, just as in etching. It has been argued that anisotropic accommodation of vacancies beyond just anisotropy in diffusion is required for this behavior.[46]

In summary, our atomistic modeling of the etching and oxidation of vicinal Si(100), while still simplifying some aspects of the process, has been quite successful in generating the main features of the evolving surface morphology as seen in STM studies. Anisotropic energetics guarantees distinct features of smooth S_A and rough S_B steps. The kinetic model recovers the fast retraction of S_B steps due to the anisotropic accommodation of DV's at step edges (favoring S_B steps). Oxide islands pin the receding step edges. S_B steps, which are not very stiff, readily bend around these creating extended fingers, one of the most dramatic features of the STM images. For higher etching rates (and also for lower T), our modeling predicts a mixed mode of etching with island nucleation on T_A terraces and step flow across T_B terraces to S_B steps. This feature was dependent on anisotropic DV diffusion. In contrast, the existence of an island nucleation regime in the MBE modeling required formation of biatomic steps with low sticking coefficients for Si adatoms (as this simplified modeling did not incorporate anisotropic diffusion).[29]

ACKNOWLEDGMENTS

This work was supported by the SciDAC Computational Chemistry Program and the Division of Chemical Sciences of the U.S. Department of Energy (USDOE). It was performed at Ames Laboratory operated by Iowa State University under Contract No. W-7405-ENG-82.

APPENDIX A: KMC ALGORITHM

Our kinetic Monte Carlo (KMC) simulation algorithm for the atomistic LG model of Sec. IV is primarily based on a Bortz-type rejection free approach,[47] where for each process occurring with a specific rate, one maintains a corresponding list of eligible species. Then, at each KMC step, one chooses randomly from entries in these lists, weighted by the appropriate rates. Thus, we maintain lists of isolated Si adatoms, divacancies, and O adatoms, and of O adatoms with one neighboring O (each of which has a distinct diffusion rate). In addition, we maintain lists of isolated and step edge addimers for each of the eight possible lateral coordinations (since the hop rate depends on this coordination).

One complication is that the hop rates for Si ad-dimers also depend on the direction of the hop, and whether it is intralayer or interlayer. Rather than maintaining separate sublists for these different possibilities (which would require significantly more book keeping), we implement these processes with the correct physical rates by accepting some degree of rejection as follows. For each of the above eight classes of ad-dimers, a (maximal) hop rate is initially assigned given by $\nu \exp[-\beta(E_{df}+n_w+n_s)]$. Then the actual move will be executed with probability of 1, $\exp[-\beta(E_{ds}-E_{df})]$, or $\exp[-1/2\beta(E_{ds}-E_{df})]$, when hops are (i) intralayer and along the direction of dimer row, (ii) intralayer and orthogonal to the dimer row, and (iii) interlayer, respectively. As described in Sec. III, we set $E_{df}=1.0$ eV and $E_{ds}=1.3$ eV. In a sense, the penalty for the initial choice diffusion barrier which may be too low is the possibility that the eventual move would be rejected.

Finally, we note that our simulations used periodic boundary conditions in the direction of the steps, and skewed periodic boundary conditions in the direction orthogonal to the steps. For the latter, an adspecies exiting from the higher terrace on the right of the simulation images in Figs. 4 and 6, or 7, will reenter on the lower terrace on the left.

APPENDIX B: OTHER MODEL REFINEMENTS

The model described in Sec. IV does not incorporate a pathway for reaction of O with isolated diffusing Si addimers (other than by depositing on top of them). This pathway which might have reduced barrier $E_{SiO}* < E_{SiO}$, could be significant as such ad-dimers are continually generated by

detachment from step edges. Such an enhanced pathway introduces an additional parameter into the model. Thus, rather than perform a comprehensive analysis of this extended model, we just consider the case where the overall reaction rate for this pathway is comparable to that of the standard pathway. We also require that the total etch rate is comparable to that in the model of Sec. IV. We then ask if there is any discernable difference in the etch morphologies?

To select parameters in the extended model to achieve the desired behavior, we note that the density per site of diffusing Si ad-dimers has the form $\exp[-\beta(\phi_w+\phi_s)]$, so the overall etch rate from reaction with these has the form $\exp[-\beta(E^*_{\mathrm{SiO}}+\phi_w+\phi_s)]$, which should be compared with $\exp[-\beta E_{\mathrm{SiO}}]$ from the standard pathway. Thus, we choose $E^*_{\mathrm{SiO}}=E_{\mathrm{SiO}}-\phi_w-\phi_s$. Since we have two comparable pathways, we also increase barriers for both pathways by a small amount to reduce the rate for each by a factor of two. Then, simulation of the extended model reveals oxide cluster density and oxygen uptake behavior essentially identical to the standard model of Sec. IV (as desired). Furthermore, examination of the etch morphologies reveals no significant difference from those of the standard model.

Next, we comment on the treatment of nucleation of oxide islands, including possible enhanced nucleation at step edges. Our treatment of oxide nucleation is somewhat *ad hoc*, and certainly more input on atomistic energetics for this process would help to refine the modeling. Nonetheless, we can reasonably describe the observed oxide island density and oxygen uptake. However, the modeling presented here has not included a mild enhancement of nucleation of oxide islands at step edges, a feature quantified in one experimental study.[37] This feature has been implemented in our modeling, but does not significantly change the behavior described in this study. Finally, we note that our modeling, similar to that of Ref. 6, does not produce the degree of saturation of the oxide island density observed in experiment. One possibility to closer match the latter would be to reduce the oxygen diffusion barrier so as to increase L_{O} to a value comparable to the observed oxide island separation as this would inhibit oxide island nucleation.

[1] T. Engel, Surf. Sci. Rep. **18**, 91 (1993).
[2] J. B. Hannon, M. C. Bartelt, N. C. Bartelt, and G. L. Kellogg, Phys. Rev. Lett. **81**, 4676 (1998).
[3] *Fundamental Aspects of Silicon Oxidation*, edited by Y. J. Chabal (Springer, Berlin, 2001).
[4] J. V. Seiple and J. P. Pelz, Phys. Rev. Lett. **73**, 999 (1994).
[5] J. V. Seiple and J. P. Pelz, J. Vac. Sci. Technol. A **13**, 772 (1995).
[6] C. Ebner, J. V. Seiple, and J. P. Pelz, Phys. Rev. B **52**, 16 651 (1995).
[7] J. V. Seiple, C. Ebner, and J. P. Pelz, Phys. Rev. B **53**, 15 432 (1996).
[8] M. A. Albao, D.-J. Liu, C. H. Choi, M. S. Gordon, and J. W. Evans, Surf. Sci. **555**, 51 (2004).
[9] M. Suemitsu, Y. Enta, Y. Miyanishi, and N. Miyamoto, Phys. Rev. Lett. **82**, 2334 (1999).
[10] K. Wurm, R. Kliese, Y. Hong, B. Rottger, Y. Wei, H. Neddermeyer, and I. S. T. Tsong, Phys. Rev. B **50**, 1567 (1994).
[11] M. C. Bartelt, J. B. Hannon, A. K. Schmid, C. R. Stoldt, and J. W. Evans, Colloids Surf., A **165**, 373 (2000).
[12] J. L. Skrobiszewski, J. C. Moore, J. W. Dickinson, and A. A. Baski, J. Vac. Sci. Technol. A **22**(R) 1667 (2004).
[13] H. Zandvliet, Rev. Mod. Phys. **72**, 593 (2000).
[14] B. Voigtlander, Surf. Sci. Rep. **43**, 127 (2001).
[15] N. C. Bartelt, R. M. Tromp, and E. D. Williams, Phys. Rev. Lett. **73**, 1656 (1994).
[16] D. J. Eaglesham, A. E. White, L. C. Feldman, N. Moriya, and D. C. Jacobson, Phys. Rev. Lett. **70**, 1643 (1993).
[17] B. S. Swartzentruber, Y.-W. Mo, R. Kariotis, M. G. Lagally, and M. B. Webb, Phys. Rev. Lett. **65**, 1913 (1990).
[18] A. Esteve, Y. J. Chabal, K. Raghavachari, M. K. Weldon, K. T. Queeney, and M. Djafari Rouhani, J. Appl. Phys. **90**, 6000 (2001).
[19] M. K. Weldon, B. B. Stefanov, K. Raghavachari, and Y. J. Chabal, Phys. Rev. Lett. **79**, 2851 (1997).
[20] Y. J. Chabal, K. Raghavachari, X. Zhang, and E. Garfunkel, Phys. Rev. B **66**, 161315(R) (2002).
[21] C. H. Choi and M. S. Gordon, in *Computational Materials Chemistry: Methods and Applications*, edited by L. A. Curtiss and M. S. Gordon (Kluwer, Dordrecht, 2004), p. 125.
[22] C. H. Choi, D.-J. Liu, J. W. Evans, and M. S. Gordon, J. Am. Chem. Soc. **124**, 8730 (2002).
[23] Y. Miyamoto and A. Oshiyama, Phys. Rev. B **41**, 12 680 (1990).
[24] Z. Zhang and H. Metiu, Phys. Rev. B **48**, 8166 (1993).
[25] Z. Zhang, F. Wu, H. J. W. Zandvliet, B. Poelsema, H. Metiu, and M. G. Lagally, Phys. Rev. Lett. **74**, 3644 (1995).
[26] B. Borovsky, M. Krueger, and E. Ganz, Phys. Rev. Lett. **78**, 4229 (1997).
[27] S. Clarke and D. D. Vvedensky, J. Appl. Phys. **63**, 2272 (1988).
[28] B. Voigtlander, T. Weber, P. Smilauer, and D. E. Wolf, Phys. Rev. Lett. **78**, 2164 (1997).
[29] N. Kitamura, M. G. Lagally, and M. B. Webb, Phys. Rev. Lett. **71**, 2082 (1993).
[30] Y. W. Mo, J. Kleiner, M. B. Webb, and M. G. Lagally, Phys. Rev. Lett. **66**, 1998 (1991).
[31] Q.-M. Zhang, C. Roland, P. Boguslawski, and J. Bernholc, Phys. Rev. Lett. **75**, 101 (1995).
[32] C. Pearson, M. Krueger, and E. Ganz, Phys. Rev. Lett. **76**, 2306 (1996).
[33] B. S. Swartzentruber, Phys. Rev. B **55**, 1322 (1997).
[34] D. G. Cahill and Ph. Avouris, Appl. Phys. Lett. **60**, 326 (1992).
[35] P. Jensen, H. Larralde, and A. Pimpinelli, Phys. Rev. B **55**, 2556 (1997).
[36] J. A. Venables, Philos. Mag. **27**, 693 (1973).
[37] V. Brichzin and J. P. Pelz, Phys. Rev. B **59**, 10 138 (1999).
[38] H.-C. Jeong and E. D. Williams, Surf. Sci. Rep. **34**, 171 (1999).
[39] J. W. Evans and M. C. Bartelt, J. Vac. Sci. Technol. A **12**, 1800 (1994).
[40] W. Theis and R. M. Tromp, Phys. Rev. Lett. **76**, 2770 (1996).
[41] The feature of our model that the direct DV diffusion pathway is inoperative for the last hop producing aggregation of DV means

the n_{DV} values are somewhat higher than if it was active.
[42] M. C. Bartelt and J. W. Evans, Europhys. Lett. **21**, 99 (1993).
[43] M. C. Bartelt, A. K. Schmid, J. W. Evans, and R. Q. Hwang, Phys. Rev. Lett. **81**, 1901 (1998).
[44] J. Myslivecek, C. Shelling, F. Schaffler, G. Springholz, P. Smilauer, J. Krug, and B. Voigtlander, Surf. Sci. **520**, 193 (2003).
[45] P. Bedrossian and T. Klitsner, Phys. Rev. Lett. **68**, 646 (1992).
[46] In our modeling, DV incorporation just at descending steps effectively provides such an additional anisotropy. However, the claim in Ref. 45 that anisotropic diffusion of vacancies and isotropic incorporation at all steps would lead to depleted T_A terraces seems unfounded.
[47] A. B. Bortz, M. H. Kalos, and J. L. Lebowitz, J. Comput. Phys. **17**, 10 (1975).